Journal of Power and Energy Engineering, 2025, 13(6), 65-75
https://www.scirp.org/journal/jpee
ISSN Online: 2327-5901
ISSN Print: 2327-588X

Core-Shell VN@PCNs Nanoreactors as Cathode Materials for High-Performance Aqueous Zinc Ion Batteries

Yiwen Wang, Tianqi Yong, Yinsong Wang, Yingqiang Yang, Xinyu Li*

College of Physics and Electronic Information Engineering, Guilin University of Technology, Guilin, China
Email: *lixinyu5260@163.com

How to cite this paper: Wang, Y.W., Yong, T.Q., Wang, Y.S., Yang, Y.Q. and Li, X.Y. (2025) Core-Shell VN@PCNs Nanoreactors as Cathode Materials for High-Performance Aqueous Zinc Ion Batteries. *Journal of Power and Energy Engineering*, **13**, 65-75.
https://doi.org/10.4236/jpee.2025.136004

Received: May 6, 2025
Accepted: June 27, 2025
Published: June 30, 2025

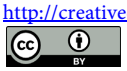

Abstract

Aqueous zinc ion water batteries (AZIBs) have attracted much attention due to their high safety, lo w cost, and environmental friendliness, but their cathode materials still face challenges in terms of volume change, reaction kinetics, and structural stability. In this study, vanadium nitride/nitrogen-doped carbon (VN@PCNs) nanoreactors with a core-shell structure were successfully constructed by encapsulating VN nanorods in porous hollow carbon spheres through a synergistic optimization strategy of interfacial engineering and structural modulation. This structure of the nanoreactor significantly reduces the dissolution and structural collapse of the active material, thus maintaining the stability of the electrode structure during multiple charge/discharge cycles. Meanwhile, the concentration gradient formed inside and outside the core-shell structure significantly enhances the diffusion of hydrated zinc ions, effectively improving the slow desolvation rate. Thanks to these advantages, the electrode can still maintain a specific capacity of up to 328 mAh g^{-1} after 500 cycles at a current density of 3 A g^{-1}, which provides a valuable research direction for the subsequent development of zinc ion batteries.

Keywords

Vanadium Nitride, Aqueous Zinc Ion Batteries, Core-Shell Structure, Nanoreactor

1. Introduction

Aqueous zinc ion batteries (AZIBs) are regarded as an ideal choice for next-generation large-scale energy storage systems due to their inherent safety and environmental friendliness, as well as the significant advantages of abundant zinc metal resources, low cost and high theoretical capacity [1]-[3]. In the exploration of

cathode materials for AZIBs, manganese-based oxides, vanadium-based compounds and Prussian blue analogs (PBAs) have been involved [4]-[6], but vanadium-based materials are one of the most popular cathode materials currently. Compared to oxygenated vanadates (V_2O_5, VO_2), which have been widely studied, oxygen-free vanadates (VN, VS_2, VC, etc.) are becoming a new research hotspot due to their inherent high electronic conductivity and higher specific capacity.

Among them, vanadium nitride (VN) is noted for its better electronic/ionic conduction properties [7]-[9]. More importantly, the microstructure of VN undergoes a dynamic evolution from an initial dense state to a loose and porous morphology during the charge/discharge cycles of AZIBs, a process that effectively increases the active sites for electrochemical reactions and contributes additional reversible capacity [10]. However, there are still serious challenges in bringing VN anodes to practical applications: first, the repeated embedding/disembedding of Zn^{2+} in the VN lattice is accompanied by significant volume changes [11] [12]. Second, in the conventional monolayer electrode structure, the strong electrostatic interactions between the ion-electrode interface hinder the ion transport efficiency and retard the critical desolvation process [13]. In addition, VN materials also suffer from dissolution loss of active substances and gradual structural collapse during long-term cycling, which together limit their cycle life and performance stability.

To overcome the above bottlenecks, researchers have explored a variety of modification strategies, such as structure and morphology modification, surface engineering, and elemental doping [14]-[16]. In recent years, the construction of protective shell layers on the surface of active materials has received increasing attention [13]. Utilizing the spatial domain-limiting effect of the shell layer not only effectively buffers the volume change of VN and maintains structural integrity but also inhibits its agglomeration and dissolution problems during the cycling process. Meanwhile, considering that Zn^{2+} in aqueous electrolytes usually exists in the form of $[Zn(H_2O)_6]^{2+}$, which has a large hydrated ion diameter (~0.86 nm) [17] [18]. Therefore, optimization of the pore structure of the protective shell layer to facilitate rapid transport and efficient desolvation of such large-sized hydrated ions is essential to enhance multiplicity performance and cycling stability.

Based on this, in this study, VN nanorods were encapsulated in porous hollow carbon spheres to construct vanadium nitride/nitrogen-doped carbon (VN@PCNs) nanoreactors with a core-shell structure through a synergistic optimization strategy of interfacial engineering and structural modulation. This structure of the nanoreactor can significantly reduce the dissolution and structural collapse of the active material, and can maintain the stability of the electrode structure during multiple charge/discharge cycles. Meanwhile, the concentration gradient difference formed inside and outside the core-shell structure significantly enhanced the diffusion ability of hydrated zinc ions. The experimental results showed that the capacity of the VN@PCNs electrode was stably maintained at 470 mAh g^{-1} after 50 short cycles at 0.1 A g^{-1} current density, and 300 mAh g^{-1} after 500 cycles at 3

A g^{-1} current density. This new cathode material not only effectively alleviates the problems caused by volume expansion and slow electrochemical kinetics, but also provides new possibilities for the commercial application of AZIBs.

2. Experimentation and Characterization

2.1. Experimental Drugs and Test Equipment

The raw materials such as vanadium acetylacetonate oxovanadium ($C_{10}H_{14}O_5V$, AR99%), isopropanol (C_3H_8O, AR), anhydrous glucose ($C_6H_{12}O_6$, AR99%), and anhydrous ethanol (C_2H_5OH, AR) were purchased commercially. In this study, TESCAN MIRALMS SEM and FEI Talos F200X G2 TEM were used to characterize the micromorphology of the electrode materials. ASAP-2460 BET was used to analyze the pore structure and the specific surface area of the materials. D8 XRD equipment was used to analyze the crystalline structure and the composition of the material phases. Thermo Scientific kalpha XPS equipment was used to analyze the elemental composition and chemical state of the materials. The related electrochemical tests were carried out on Shanghai Chenhua CHI760E electrochemical workstation.

2.2. Preparation of Electrode Materials

In a typical synthesis, 0.3 g of vanadium acetylacetonate was dissolved in 35 mL of isopropanol, and 0.1 g of anhydrous glucose was slowly added to the solution after stirring for 1 h. The mixture was vigorously stirred for 2 h and then transferred to a polytetrafluoroethylene reactor for 24 h at 200˚C. After stirring vigorously for 2 h, the mixed solution was transferred to a polytetrafluoroethylene reactor and hydrothermally reacted at 200˚C for 24 h. A lime green precipitate was obtained and centrifuged, washed three times with anhydrous ethanol and deionized water, and then dried in a vacuum oven at 70˚C overnight. The dried product was calcined at 700˚C for 2 h (heating rate: 5˚C min^{-1}) under flowing nitrogen. After cooling to room temperature, the VN@PCNs samples were obtained. The control sample was commercial vanadium nitride.

2.3. Electrode Preparation and Battery Assembly

In this study, a 3 M Zn $(CF_3SO_3)_2$ electrolyte was used to test the storage performance of Zn^{2+} in VN@CNS/CNF composites in a CR2016 coin cell. The battery configuration used zinc as the negative electrode and a glass fiber membrane as the diaphragm. The negative electrode was prepared by mixing the synthesized active material (VN@CNS/CNF), conductive agent (Super-P) and polyvinylidene fluoride in N-methyl-2-pyrrolidone at a mass ratio of 7:2:1 for 30 min. The mixture was thoroughly milled to form a homogeneous slurry, which was then uniformly coated on a stainless steel mesh and vacuum-dried at 60˚C for 18 h. The active material loading on the electrodes was maintained at about 2 mg cm^{-2}. The cathode wafers, diaphragm, electrolyte, and zinc flakes were sequentially loaded into the battery case and encapsulated using a sealing machine. Subsequently, the

cells were activated at room temperature for 12 h and then tested for electrochemical performance.

3. Results and Analysis

3.1. Characterization of Materials

In order to comprehensively characterize the microstructure and elemental composition of the VN@PCNs composites, the samples were observed by field emission scanning electron microscopy (SEM) in this study, and the samples exhibited typical porous core-shell spherical structural features as shown in Figures 1(a)-(c). The high-magnification SEM images show that the surface shell layer of the composite has an obvious rough morphology and is distributed with dense nanoscale pores, and this unique structural feature provides an ideal transport channel for the rapid diffusion of hydrated zinc ions. The synergistic effect of the porous structure not only significantly enhances the desolvation efficiency of Zn^{2+}, but also optimizes the ion storage performance to achieve rapid and directional ion transport. TEM images show that the core-shell interface is clearly visible, which provides sufficient buffer space for volume expansion during the cycling process, and this structural feature is conducive to the improvement of the electrochemical stability and cycling performance of the material. In order to verify the elemental composition and distribution characteristics of the materials, energy dispersive X-ray diffraction (EDS) analysis was carried out in this study, and the EDS map (Figure 1(d)) confirms the homogeneous distribution of nitrogen (N), vanadium (V), and carbon (C) elements in the composites.

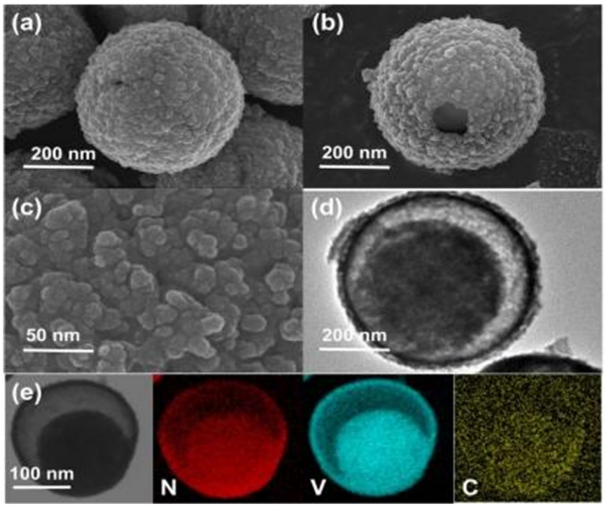

Figure 1. (a)-(c) Scanning electron microscope images of VN@PCNs; (d) Scanning electron microscope images of VN@PCNs; (e) EDS elemental maps of VN@PCNs.

In order to investigate the crystal structure of VN@PCNs composites, they were characterized by XRD in this study. As shown in Figure 2(a), the XRD pattern presents clear diffraction peaks at 37.7˚, 43.7˚, 63.6˚, 76.4˚, and 80.3˚, which correspond to the (111), (200), (220), (311), and (222) crystallographic

facets of vanadium nitride (VN), respectively (JCPDS No. 35-0768). The observation of a broad peak near 25˚ attributable to the (002) crystalline facet of amorphous graphitic carbon and the absence of impurity peaks in the plots indicate that the prepared composites are of high purity. To further evaluate the structural characteristics of the VN@PCNs samples, Raman spectroscopy was performed, testing the range from 0 to 2500 cm^{-1}. As shown in **Figure 2(b)**, the Raman spectroscopy results confirmed the presence of V-N and V-O bonds in the samples, thus validating the successful construction of the expected chemical structures. In order to fully understand the pore properties of the synthesized materials, nitrogen physisorption tests were performed in this study. As shown in **Figure 2(c)** and **Figure 2(d)**, the VN@PCNs material exhibits a typical mesoporous structure. The adsorption isotherms in the range of relative pressure (P/P_0) of 0.043 - 1.0 showed Langmuir IV-type characteristics and exhibited an obvious hysteresis loop. This phenomenon indicates that the material has a well-developed mesoporous structure and high porosity, which enables the electrolyte to contact the electrode material more fully and accelerates the kinetic process of the electrochemical reaction.

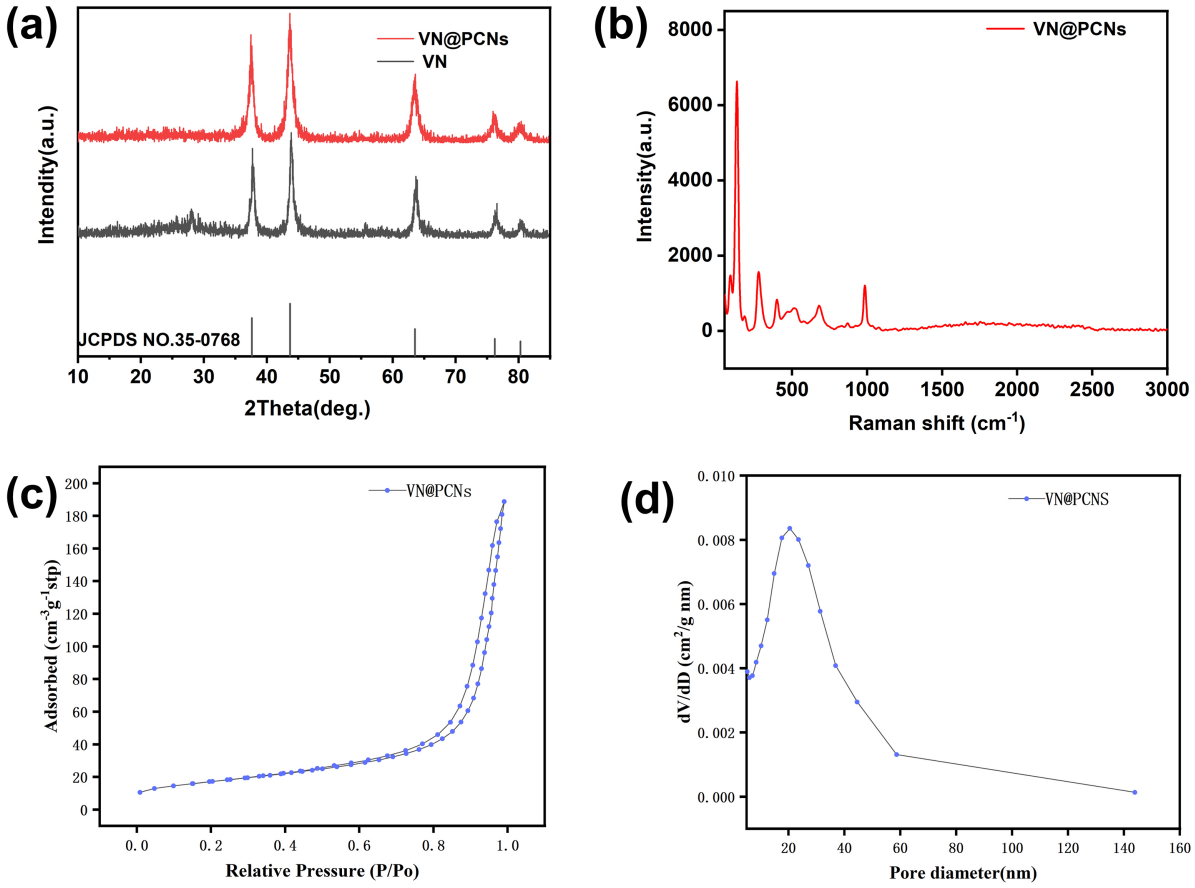

Figure 2. (a) XRD plots of VN@PCNs and VN; (b) Raman spectra of VN@PCNs; (c) N_2 adsorption/desorption isotherms of VN@PCNs; (d) corresponding pore size distributions of VN@PCNs.

X-ray photoelectron spectroscopy (XPS) analysis was used to probe deeply into the chemical composition and valence information of the VN/N-C composite. The full spectrum (**Figure 3(a)**) clearly reveals the presence of three elements, V, N and C, in the composite. However, due to the easy oxidation of metal nitrides in air, M-O species are formed on their surfaces [19] [20], which is attributed to the fact that the activation process enhances the phase transition efficiency and thus the utilization of active materials [21]. The N 1s high-resolution spectrum (**Figure 3(b)**) presents three characteristic peaks located at 401.8 eV (V-N-O bond), 399.9 eV (N-C bond) and 397.4 eV (V-N bond).The V 2p spectrum (**Figure 3(c)**) presented three peaks at 517.6 eV, 516.5 eV, and 514.1 eV, which were attributed to V-O, V-N-O, and V-N bonds, respectively [22]. The high-resolution C 1s spectra of VN/N-C (**Figure 3(d)**) with three characteristic peaks located at 284.8 eV, 286.3 eV, and 289.0 eV correspond to C-C, C-O, and C=O bonds, respectively. These XPS analysis results are highly consistent with the Raman spectroscopy findings.

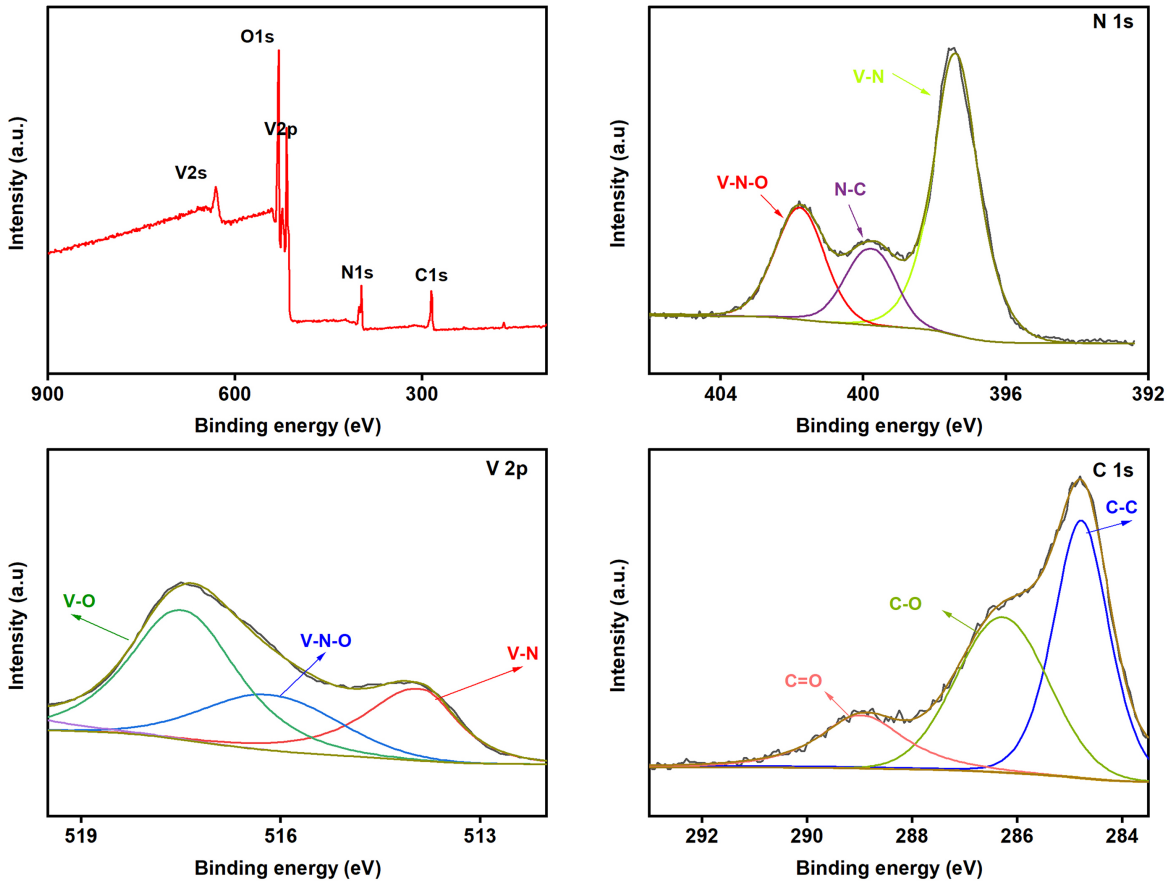

Figure 3. (a) Full scanning X-ray photoelectron spectra of the composites of VN/N-C composites; (b) N 1s; (c) V 2p; (d) C 1s.

3.2. Electrochemical Performance Testing

The electrochemical performance of the VN@PCNs electrode was systematically

evaluated in this study through constant-current charge/discharge tests. As shown in Figure 4(a), the electrode maintains stable electrochemical performance after 50 cycles at 0.1 A g^{-1} current density, and its reversible capacity is always maintained around 470 mAh g^{-1}, demonstrating good cycling stability. Figure 4(b) reveals the excellent multiplicative performance of the VN@PCNs electrode. With the gradual increase of the test current density from 0.1 A g^{-1} to 0.2 A g^{-1}, 0.5 A g^{-1}, 1 A g^{-1}, and 2 A g^{-1}, the reversible discharge specific capacity of the VN@PCNs electrodes, although somewhat decreased, still exhibited high efficiency, reaching 470 mAh g^{-1}, 426 mAh g^{-1}, 406 mAh g^{-1}, 386 mAh g^{-1} and 348mAh g^{-1}, respectively. In contrast, the discharge-specific capacity of VN electrodes under the same conditions is relatively low. To evaluate the long-term performance of the VN@PCNs electrode, the present study achieved a capacity of 336 mAh g^{-1} at a high current density of 3 Ag^{-1}, and maintained a high specific capacity of 328 mAh g^{-1} after 500 charge/discharge cycles. This result fully confirms the excellent structural stability and electrochemical reversibility of VN@PCNs composites during long-term cycling.

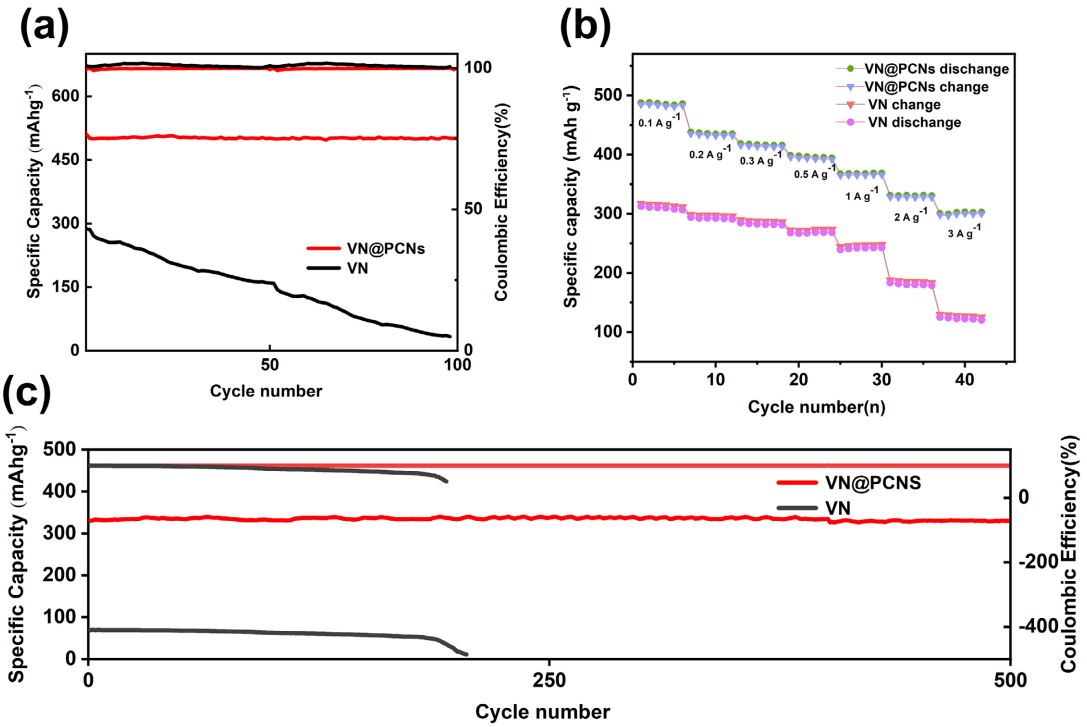

Figure 4. (a) CV curves at a scan rate of 0.1 1 mV s^{-1}; (b) multiplicative performance at different current densities; (c) long-term cycling stability at a high current density of 3 A g^{-1}.

In order to elucidate the electrochemical response characteristics of the VN@PCNs electrodes, their cyclic voltammetric curves were investigated in the range of 0.1 - 1.0 mV s^{-1} scan rate. As shown in Figure 5(a), the VN@PCNs composites exhibit significant advantages in terms of electrochemical reversibility, cycling stability, and multiplicity performance compared with the VN electrodes. With the in-

crease in scanning rate, the electrode polarization phenomenon gradually intensified, which was manifested by a positive shift of the oxidation peak potential, while the reduction peak potential showed a negative shifting trend. This characteristic potential shift phenomenon is closely related to the charge transport kinetic process inside the electrode material. The capacity contribution pattern is determined by applying the kinetic equation containing the peak current (i) and scan rate (υ) [23]:

$$i = a\upsilon^b \tag{1}$$

where b values close to 0.5 indicate diffusion-controlled processes, while b values close to 1.0 indicate that the underlying mechanism is mainly non-diffusion-controlled. As shown in **Figure 5(b)**, the b-values of the four redox peaks are 0.69, 0.73, 0.68, and 0.72, respectively, which indicates that surface-induced pseudocapacitance plays an important role in the overall capacity. The ratio of Zn^{2+} capacitance contribution ($k_1 v$) to diffusion contribution ($k_2 v$) in the overall capacity at a specific scan rate [24]:

$$i = k_1 v + k_2 \upsilon^{1/2} \tag{2}$$

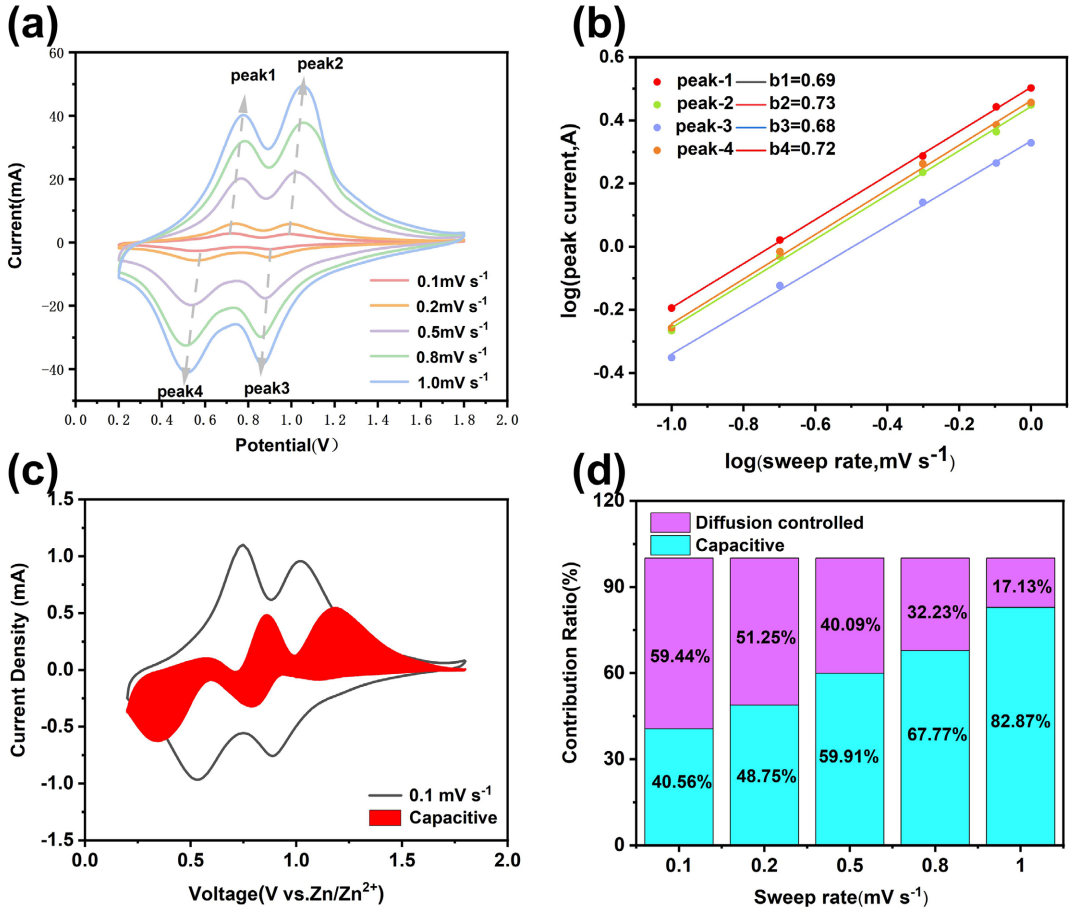

Figure 5. (a) CV curves at different scan rates; (b) plot of log(i) versus log(v) based on the CV data to investigate the relationship between the redox peaks and the scan rate; (c) capacitance separation curves for a scan rate of 0.1 mV s^{-1}; (d) analysis of the contribution of the capacitive behavior to the overall capacity at different scan rates.

At a scan rate of 0.1 mV s^{-1}, the capacitive contribution was 40.56% of the total capacity (Figure 5(c)). As the scan rate increases, the capacitive contribution also increases from 40.56% to 82.87% (Figure 5(d)). The experimental results show that the pseudocapacitance contribution shows a steady increase as the scan rate increases, while the pseudocapacitance contribution gradually dominates. This suggests that the surface redox reaction plays a more critical role in promoting the reversible embedding/de-embedding of Zn^{2+} ions compared to the controlled process limited by the diffusion in the bulk phase of the material.

In order to investigate the electrochemical kinetic properties of the electrode materials deeply, the electrochemical impedance spectroscopy (EIS) technique was used in this study to systematically characterize the VN@PCNs and VN samples. As shown in Figure 6, the impedance of VN@PCNs and VN was evaluated by EIS. The equivalent circuit model analyzed by EIS shows that the charge transfer impedance of VN@PCNs is 153.1 Ω, which is significantly lower than that of VN under the same condition, which is 386.3 Ω. The decrease in impedance suggests that the porous nitrogen-doped carbon shell of VN in the structure of VN@PCNs significantly improves the charge transfer kinetics.

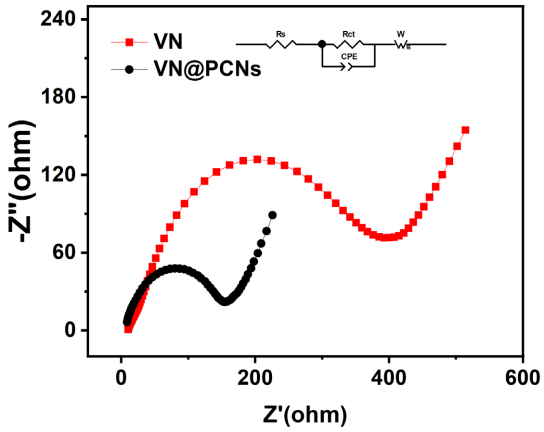

Figure 6. EIS spectra were fitted to an equivalent circuit model.

4. Conclusion

In this paper, the template-free solvothermal method is combined with a high-temperature nitriding process to encapsulate VN nanorods in porous hollow carbon spheres through a synergistic optimization strategy of interfacial engineering and structural modulation to construct vanadium nitride/nitrogen-doped carbon (VN@PCNs) nanoreactors with core-shell structure. The nanoreactor can significantly reduce the dissolution and structural collapse of the active material, and can maintain the stability of the electrode structure during multiple charge/discharge cycles. Meanwhile, the concentration gradient difference formed inside and outside the core-shell structure significantly enhanced the diffusion ability of hydrated zinc ions and improved the slow desolvation rate. The results show that the porous core-shell VN@PCNs composites maintain a high specific capacity of

300 mAh g^{-1} after 500 cycles at a current density of 3 A g^{-1}. This study provides a valuable research direction for the subsequent development of zinc ion batteries.

Conflicts of Interest

The authors declare no conflicts of interest regarding the publication of this paper.

References

[1] Lv, Y., Xiao, Y., Ma, L., Zhi, C. and Chen, S. (2021) Recent Advances in Electrolytes for "Beyond Aqueous" Zinc-Ion Batteries. *Advanced Materials*, **34**, Article 2106409. https://doi.org/10.1002/adma.202106409

[2] Yuan, Y., Wu, S., Song, X., Lee, J.Y. and Kang, B. (2023) Recent Progress and Regulation Strategies of Layered Materials as Cathode of Aqueous Zinc-Ion Batteries. *Energy & Environmental Materials*, **7**, e12632. https://doi.org/10.1002/eem2.12632

[3] Zhao, J., Wang, Q., Tan, F., Liu, Y., Xue, X., Li, M., *et al.* (2023) Highly Flexible and Compressible Zinc-Ion Batteries with Superb Electrochemical Performance Enabled by a Dual Structural Regulation Strategy. *Energy Storage Materials*, **56**, 478-488. https://doi.org/10.1016/j.ensm.2023.01.040

[4] Zhang, N., Cheng, F., Liu, Y., Zhao, Q., Lei, K., Chen, C., *et al.* (2016) Cation-Deficient Spinel $ZnMn_2O_4$ Cathode in $Zn(CF_3SO_3)_2$ Electrolyte for Rechargeable Aqueous Zn-Ion Battery. *Journal of the American Chemical Society*, **138**, 12894-12901. https://doi.org/10.1021/jacs.6b05958

[5] Xia, J., Zhou, Y., Zhang, J., Lu, T., Gong, W., Zhang, D., *et al.* (2023) Triggering High Capacity and Superior Reversibility of Manganese Oxides Cathode via Magnesium Modulation for Zn//MnO_2 Batteries. *Small*, **19**, Article 2301906. https://doi.org/10.1002/smll.202301906

[6] Liu, Y., Liu, Y., Wu, X. and Cho, Y. (2022) Enhanced Electrochemical Performance of Zn/VO_x Batteries by a Carbon-Encapsulation Strategy. *ACS Applied Materials & Interfaces*, **14**, 11654-11662. https://doi.org/10.1021/acsami.2c00001

[7] Wang, T., Sun, J., Hua, Y., Krishna, B.N.V., Xi, Q., Ai, W., *et al.* (2022) Planar and Dendrite-Free Zinc Deposition Enabled by Exposed Crystal Plane Optimization of Zinc Anode. *Energy Storage Materials*, **53**, 273-304. https://doi.org/10.1016/j.ensm.2022.08.046

[8] Chen, X., Sun, W. and Wang, Y. (2020) Covalent Organic Frameworks for Next-Generation Batteries. *ChemElectroChem*, **7**, 3905-3926. https://doi.org/10.1002/celc.202000963

[9] Shuai, H., Xu, J. and Huang, K. (2020) Progress in Retrospect of Electrolytes for Secondary Magnesium Batteries. *Coordination Chemistry Reviews*, **422**, Article 213478. https://doi.org/10.1016/j.ccr.2020.213478

[10] Han, J., Yang, J., Xu, Z., Li, H. and Wang, J. (2022) Dramatic Improvement in High-Rate Capability of LiMnPO4 Nanosheets via Crystallite Size Regulation. *Journal of Alloys and Compounds*, **894**, Article 162510. https://doi.org/10.1016/j.jallcom.2021.162510

[11] Wan, F., Zhang, L., Dai, X., Wang, X., Niu, Z. and Chen, J. (2018) Aqueous Rechargeable Zinc/Sodium Vanadate Batteries with Enhanced Performance from Simultaneous Insertion of Dual Carriers. *Nature Communications*, **9**, Article No. 1656. https://doi.org/10.1038/s41467-018-04060-8

[12] Yang, H., Ning, P., Wen, J., Xie, Y., Su, C., Li, Y., *et al.* (2021) Structure Control in

VN_xO_y by Hydrogen Bond Association Extraction for Enhanced Zinc Ion Storage. *Electrochimica Acta*, **389**, Article 138722. https://doi.org/10.1016/j.electacta.2021.138722

[13] Long, Y., An, X., Yang, Y., Yang, J., Liu, L., Tong, X., *et al.* (2025) Gradient Porous Carbon Superstructures for High-Efficiency Charge Storage Kinetics. *Advanced Functional Materials*, Article 2424551. https://doi.org/10.1002/adfm.202424551

[14] Zhang, Y., Chen, A. and Sun, J. (2021) Promise and Challenge of Vanadium-Based Cathodes for Aqueous Zinc-Ion Batteries. *Journal of Energy Chemistry*, **54**, 655-667. https://doi.org/10.1016/j.jechem.2020.06.013

[15] Zhang, W., Liang, S., Fang, G., Yang, Y. and Zhou, J. (2019) Ultra-High Mass-Loading Cathode for Aqueous Zinc-Ion Battery Based on Graphene-Wrapped Aluminum Vanadate Nanobelts. *Nano-Micro Letters*, **11**, Article No. 69. https://doi.org/10.1007/s40820-019-0300-2

[16] Liu, Y., Li, Q., Ma, K., Yang, G. and Wang, C. (2019) Graphene Oxide Wrapped CuV_2O_6 Nanobelts as High-Capacity and Long-Life Cathode Materials of Aqueous Zinc-Ion Batteries. *ACS Nano*, **13**, 12081-12089. https://doi.org/10.1021/acsnano.9b06484

[17] Wang, N., Zhang, W., Li, Z., Wang, S., Suwardi, A., Ye, E., *et al.* (2022) Dual-Electric-polarity Augmented Cyanoethyl Cellulose-Based Triboelectric Nanogenerator with Ultra-High Triboelectric Charge Density and Enhanced Electrical Output Property at High Humidity. *Nano Energy*, **103**, Article 107748. https://doi.org/10.1016/j.nanoen.2022.107748

[18] Li, X., Lin, Z., Jin, N., Yang, X., Du, Y., Lei, L., *et al.* (2021) Perovskite-Type $SrVO_3$ as High-Performance Anode Materials for Lithium-Ion Batteries. *Advanced Materials*, **34**, Article 2107262. https://doi.org/10.1002/adma.202107262

[19] Li, S., Zhuang, Z., Xia, L., Zhu, J., Liu, Z., He, R., *et al.* (2023) Improving the Electrophilicity of Nitrogen on Nitrogen-Doped Carbon Triggers Oxygen Reduction by Introducing Covalent Vanadium Nitride. *Science China Materials*, **66**, 160-168. https://doi.org/10.1007/s40843-022-2116-3

[20] Xie, X., Fang, G., Xu, W., Li, J., Long, M., Liang, S., *et al.* (2021) *In Situ* Defect Induction in Close-Packed Lattice Plane for the Efficient Zinc Ion Storage. *Small*, **17**, Article 2101944. https://doi.org/10.1002/smll.202101944

[21] Luo, H., Wang, B., Wu, F., Jian, J., Yang, K., Jin, F., *et al.* (2021) Synergistic Nanostructure and Heterointerface Design Propelled Ultra-Efficient *In-Situ* Self-Transformation of Zinc-Ion Battery Cathodes with Favorable Kinetics. *Nano Energy*, **81**, Article 105601. https://doi.org/10.1016/j.nanoen.2020.105601

[22] Yang, X., Chen, S., Gong, W., Meng, X., Ma, J., Zhang, J., *et al.* (2020) Kinetic Enhancement of Sulfur Cathodes by N-Doped Porous Graphitic Carbon with Bound VN Nanocrystals. *Small*, **16**, Article 2004950. https://doi.org/10.1002/smll.202004950

[23] Chen, D., Lu, M., Li, L., Cai, D., Li, J., Cao, J., *et al.* (2019) Hierarchical Core-Shell Structural $NiMoO_4$@NiS_2/MoS_2 Nanowires Fabricated *via* an *in Situ* Sulfurization Method for High Performance Asymmetric Supercapacitors. *Journal of Materials Chemistry A*, **7**, 21759-21765. https://doi.org/10.1039/c9ta07731f

[24] Zhang, K., Hu, Z., Liu, X., Tao, Z. and Chen, J. (2015) $Fese_2$ Microspheres as a High-Performance Anode Material for Na-Ion Batteries. *Advanced Materials*, **27**, 3305-3309. https://doi.org/10.1002/adma.201500196